International Journal of Nanomedicine

Dovepress

open access to scientific and medical research

Open Access Full Text Article

ORIGINAL RESEARCH

Dual-Nozzle 3D Printed Nano-Hydroxyapatite Scaffold Loaded with Vancomycin Sustained-Release Microspheres for Enhancing Bone Regeneration

Jianyi Li[1,*], Keke Li[2,*], Yukun Du[1,*], Xiaojie Tang[3,*], Chenjing Liu[1], Shannan Cao[3], Baomeng Zhao[2], Hai Huang[3], Hongri Zhao[3], Weiqing Kong[1], Tongshuai Xu[3], Cheng Shao[1], Jiale Shao[1], Guodong Zhang[4], Hongbo Lan[5], Yongming Xi[1]

[1]Department of Orthopaedic Surgery, the Affiliated Hospital of Qingdao University, Qingdao, People's Republic of China; [2]Yantai Campus of Binzhou Medical University, Yantai, People's Republic of China; [3]Yantai Affiliated Hospital of Binzhou Medical University, Yantai, People's Republic of China; [4]Tengzhou Central People's Hospital, Tengzhou, People's Republic of China; [5]Shandong Engineering Research Center for Additive Manufacturing Qingdao University of Technology, Qingdao, People's Republic of China

*These authors contributed equally to this work

Correspondence: Yongming Xi, Department of Orthopaedic Surgery, the Affiliated Hospital of Qingdao University, Qingdao, 266071, People's Republic of China, Email xym700118@163.com; Hongbo Lan, Shandong Engineering Research Center for Additive Manufacturing Qingdao University of Technology, Qingdao, 266520, People's Republic of China, Email hblan99@126.com

Background: Successful treatment of infectious bone defect remains a major challenge in the orthopaedic field. At present, the conventional treatment for infectious bone defects is surgical debridement and long-term systemic antibiotic use. It is necessary to develop a new strategy to achieve effective bone regeneration and local anti-infection for infectious bone defects.

Methods: Firstly, vancomycin / poly (lactic acid-glycolic acid) sustained release microspheres (VAN/PLGA-MS) were prepared. Then, through the dual-nozzle 3D printing technology, VAN/PLGA-MS was uniformly loaded into the pores of nano-hydroxyapatite (n-HA) and polylactic acid (PLA) scaffolds printed in a certain proportion, and a composite scaffold (VAN/MS-PLA/n-HA) was designed, which can not only promote bone repair but also resist local infection. Finally, the performance of the composite scaffold was evaluated by in vivo and in vitro biological evaluation.

Results: The in vitro release test of microspheres showed that the release of VAN/PLGA-MS was relatively stable from the second day, and the average daily release concentration was about 15.75 μg/mL, which was higher than the minimum concentration specified in the guidelines. The bacteriostatic test in vitro showed that VAN/PLGA-MS had obvious inhibitory effect on Staphylococcus aureus ATCC-29213. Biological evaluation of VAN/MS-PLA/n-HA scaffolds in vitro showed that it can promote the proliferation of adipose stem cells. In vivo biological evaluation showed that VAN/MS-PLA/n-HA scaffold could significantly promote bone regeneration.

Conclusion: Our research shows that VAN/MS-PLA/n-HA scaffolds have satisfying biomechanical properties, effectively inhibit the growth of Staphylococcus aureus, with good biocompatibility, and effectiveness on repairing bone defects. The VAN/MS-PLA/n-HA scaffold provide the clinic with an application prospect in bone tissue engineering.

Keywords: osteogenesis, dual-nozzle 3D printing technology, drug-loaded microspheres, vancomycin, nano-hydroxyapatite

Introduction

Bone defects, which are the most common problems encountered by orthopaedic surgeons, are mainly caused by trauma, infection, tumours, and degeneration, and they often manifest as pain at the defect site, limb dysfunction, and so on, which seriously affect patient quality of life.[1–3] As the bone tissue has a certain ability to regenerate, most fractures or minor bone defects can gradually recover without intervention; however, if the bone defect is too large and exceeds the

Received: 21 October 2022
Accepted: 24 December 2022
Published: 18 January 2023

Graphical Abstract

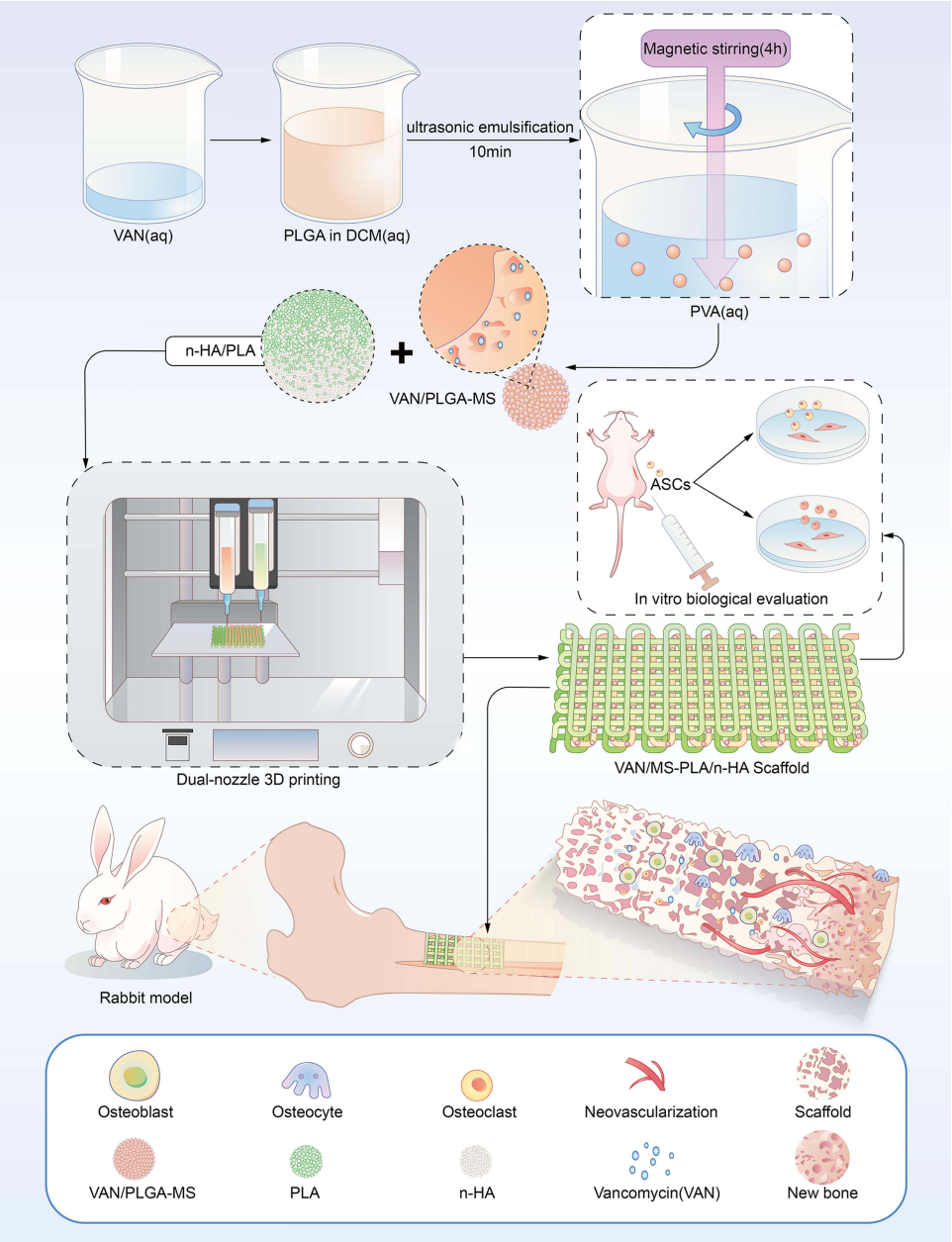

'critical range of bone defects', it cannot heal itself and must be repaired and reconstructed.[4,5] According to statistics, more than 500,000 patients need bone transplants each year in the United States alone, second only to blood cell transplants.[6,7] In addition, the large bone defects are often accompanied by a high risk of infection.[8] Pathogenic bacteria can significantly destroy local tissue and bone regeneration ability, causing local blood damage and osteonecrosis, systemic application of antibiotics is difficult to achieve effective drug concentration at the infected site, which delayed bone healing, nonunion or even amputation.[9–11] At present, the clinical materials for repairing bone defects include not only autogenous bone but also some artificial materials, such as metal titanium mesh, polyether ether ketone (PEEK), and allogeneic freeze-dried bone.[12–14] However, these traditional treatment techniques have many disadvantages, such as limited sources of autogenous bone, expensive metal and other materials, significant differences in elastic modulus

between artificial bone and human bone, and non-degradation. In addition, the current artificial materials only play a supporting role; they do not have a therapeutic effect according to the characteristics of local lesions. To ensure a good prognosis, the development of methods for reducing the treatment cycle, improving the quality of life, and reducing medical costs has become an urgent problem to be solved in the field of orthopaedic surgery.[6,15–18]

Charles Hull first invented three-dimensional (3D) lithography in 1986, and thus 3D printing has a history of more than 30 years.[19] With the rapid development of technology, biological 3D printing, with the aid of computer-aided design (CAD) technology, can accurately distribute biomaterials with cells, matrices, bioactive factors, or other functional substances to imitate the structure of natural bone tissue. Compared with monolayers, 3D printing more closely recapitulates the characteristics of natural tissue, and thus it can maintain or promote cell function to achieve more physiologically relevant results.[20–22] Because of its excellent customization, controllability and repeatability in the preparation of layered structures, 3D printing has aroused more researchers' strong research interest and has been applied worldwide.[23–25] Therefore, bone tissue engineering products are expected to become substitutes for bone tissue for clinical use in the future.

To explore the use of biodegradable engineered bone with easily available materials, an elastic modulus similar to that of natural bone, good biocompatibility, and long-lasting and effective drug release to the surrounding tissue, we integrated anti-infection properties, repair, and reconstruction of infectious bone defects. First, prepared poly (lactic-co-glycolic acid) drug microspheres containing vancomycin (VAN/PLGA-MS) with long-term sustained release were designed and developed. Next, a porous PLA/n-HA scaffold was prepared. Using dual-nozzle 3D printing technology to print the scaffold material, VAN/PLGA-MS was loaded into the pores of the engineered bone to obtain a VAN/MS-PLA/n-HA composite scaffold. Finally, the structural morphology, mechanical properties, cytocompatibility, in vitro drug release, and bacteriostatic properties of the composite scaffold were evaluated. Then, the scaffold was implanted in animals to evaluate its systemic toxicity and osteogenic properties. Vancomycin is considered as the "last resort" for the treatment of severe infection caused by Gram-positive bacteria,[26] and it has an effective bactericidal ability against methicillin-resistant Staphylococcus aureus, the most common pathogen causing blood infections in hospitalized patients.[27] Nano-hydroxyapatite is the main component of bone minerals, which is biocompatible with the physiological environment,[28] and can stimulate macrophages to secrete angiogenesis and osteogenic growth factors.[29] This kind of drug-loaded microsphere composite scaffold can be used to repair infectious bone defects.

Materials and Methods

Preparation of PLGA/VAN-MS by Orthogonal Optimisation Method

In this study, PLGA/VAN-MS was prepared using the compound emulsion solvent evaporation method (W/O/W). A certain mass of VAN solution (VIANEX S.A., Greece) was added to a DCM (Dichloromethane, Sinopharm Chemical Reagent Co., Ltd., China) solution containing PLGA (Shanghai Yuanye Bio-Technology Co., Ltd., China) and emulsified in an ice bath. The obtained colostrum was injected dropwise into 40 mL of a PVA solution (Acros, Belgium) with a certain concentration at a constant speed, and stirred in a blender at a constant speed for 4 h. The obtained compound emulsion was left for 1 h, washed, centrifuged twice, and then pre-frozen and frozen to prepare the VAN/PLGA microspheres.

Four factors that have great influence on the preparation of microspheres were included. Drug efficiency (DE%) and entrapment efficiency (EE%) were used as optimisation indexes. See Table 1.

Table 1 Experimental Factors and Level

Level	Factor A VAN (mg)	Factor B PLGA (mg)	Factor C PVA (%)	Factor D Rotational Speed (r/Min)
1	100	300	2	600
2	200	400	2.5	900
3	300	500	3	1200

Characterisation and Determination of DE% and EE% of VAN/PLGA Microspheres After Process Optimization

The particle sizes of the microspheres were measured using a Marvel 3000 particle-size analyser (Malvern Instruments Co., Ltd., Britain). A certain number of microspheres was used to observe the micromorphology under scanning electron microscopy (SEM).

Dried VAN/PLGA microspheres (10 mg) were placed in a test tube, and 1 mL of DCM was added to fully dissolve them. Then, 4 mL of phosphate-buffered saline (PBS) solution was added to the test tube. After mixing, the mixture was allowed to stand for 10 min. It was then centrifuged at 6000 rpm for 5 min. The optical density (OD) value of the supernatant at 280 nm was measured using an ultraviolet spectrophotometer. The DE% and EE% values of the microspheres were calculated using the following formulas:[30]

$$\mathrm{DE\%} = (\text{drug loading of microspheres}/\text{total mass of microspheres}) \times 100\%$$

$$\mathrm{EE\%} = (\text{actual drug loading}/\text{ideal drug loading}) \times 100\%$$

In vitro Release Test of VAN/PLGA-MS

Three scaffolds of VAN/PLGA-MS (100 mg) and standard VAN (100 mg) were added to 50 mL of PBS and placed in a constant-temperature shaker at 37 °C and 100 rpm. At 0, 1, 3, 6, 9, 12 and 24h, and at 3, 6, 9, 12, 15, 18, 21 and 24d, 4mL PBS solution was taken out for testing. Fresh PBS (4 mL) was added each time to replace the amount removed. The OD value at 280 nm was measured using a spectrophotometer, and the average value was used to calculate the cumulative drug release and sustained-release rate.

Bacteriostatic Test of PLGA-MS in vitro

Three scaffolds of dried PLGA/VAN-MS (10 mg) were placed in solid media containing ATCC-25923 Staphylococcus aureus (Yantai Affiliated Hospital of Binzhou Medical College, China) and incubated for 24 h, after which the diameter of the bacteriostatic zone was observed.

Design and Construction of Composite Scaffold

The print model of the n-HA/PLA scaffold was designed using CAD drawing software. The specifications were dimensions of 3 × 2 × 0.3 cm, linewidth 400 μm, aperture 500 μm. The overall offset of each scaffold was 100 μm higher than that of the upper scaffold (Figure S1). n-HA (Shanghai Yuanye Bio-Technology Co., Ltd., China) and PLA (Shanghai Acmec Biochemical Co., Ltd., China) powders were uniformly mixed at a mass ratio of 1:9. VAN/PLGA-MS (1 g) was uniformly dispersed in 10 mL of chitosan hydrogel containing 400 μL of Tween® 80, and the printing rate was 12 mm/s. See Figure S1 for the printing process. In the control group, a hot-melt sprinkler was used to print the scaffold material but not the drug microspheres.

Morphological Observation of Two Groups of Scaffolds

The general appearance of the n-HA/PLA and VAN/MS-PLA/n-HA scaffolds and the micromorphology of the two groups of composite scaffolds were observed using SEM.

Determination of Scaffold Porosity

The porosity of the scaffold was determined according to Archimedes' principle:[31]

$$\mathrm{P} = (\mathrm{V1} - \mathrm{V3})/(\mathrm{V2} - \mathrm{V1}) \times 100\%$$

where P is the porosity of the scaffold, $V1$ is the amount of anhydrous ethanol in the vector cylinder, $V2$ is to put the scaffold into the measuring cylinder containing anhydrous ethanol, and the volume of anhydrous ethanol is removed by ultrasonic, and $V3$ is the volume of anhydrous ethanol remaining in the cylinder after the sample of the scaffold immersed in anhydrous ethanol was removed. Therefore, $V1 - V3$ is the total pore volume of the scaffold, and $V2 - V1$ is the total

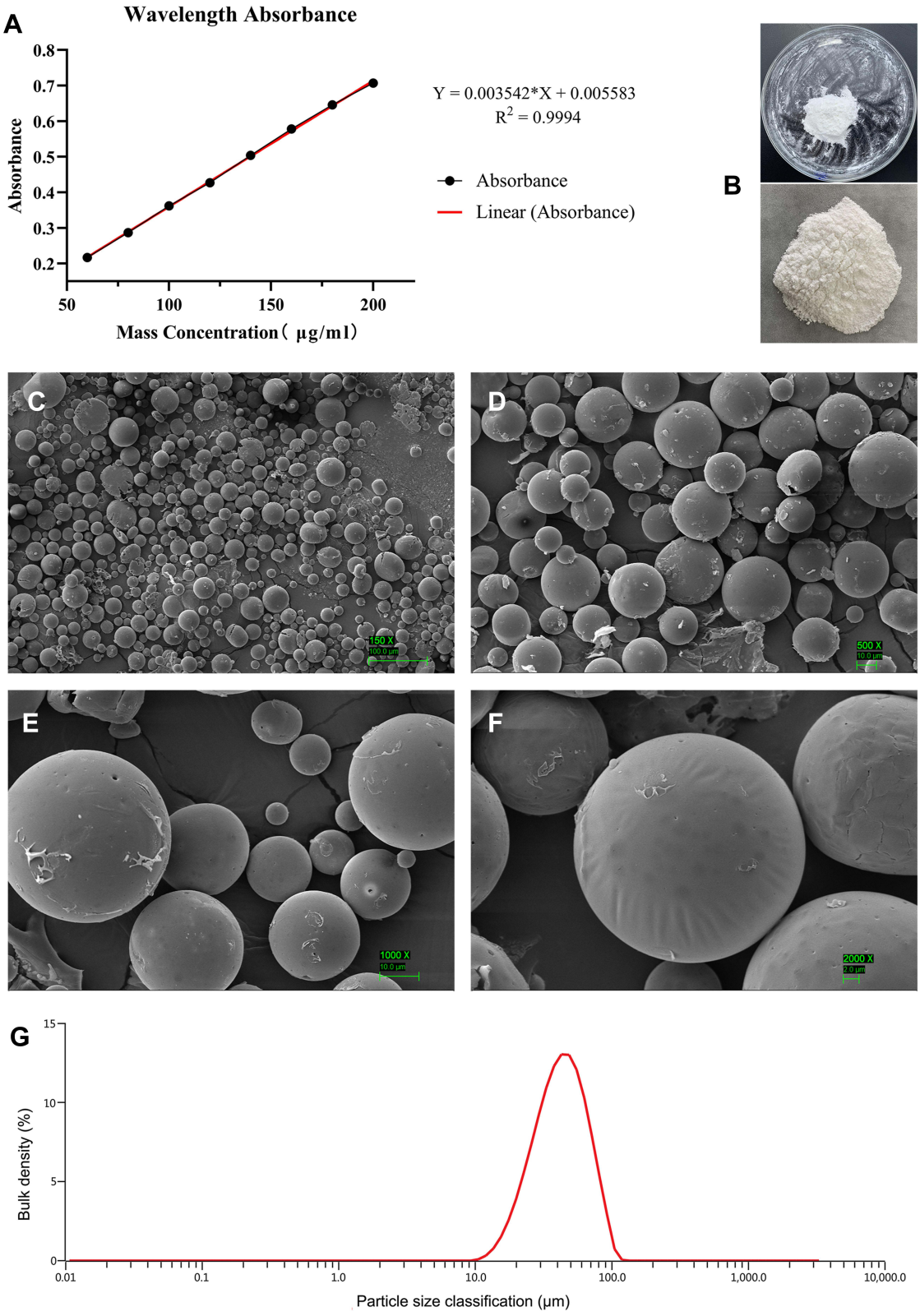

Figure 1 Characterisation of VAN/PLGA microspheres. (**A**) The standard release curve of VAN. (**B**) Macroscopic images of successfully prepared microspheres. (**C**–**F**) SEM images of the microspheres under different magnifications (150×, 500×, 1000×, 2000×, respectively). (**G**) Size distribution of microspheres.

Table 2 Orthogonal Test Table

Test Number	Factor				Observation Index		
	A (VAN)	B (PLGA)	C (PVA)	D (r)	DE%	EE%	80%DE+20%EE
1	1	1	1	1	21.731	86.923	34.7694
2	1	2	2	2	17.123	85.616	30.8216
3	1	3	3	3	13.322	79.93	26.6436
4	2	1	2	3	25.796	64.49	33.5348
5	2	2	3	1	15.768	47.304	22.0752
6	2	3	1	2	22.719	79.518	34.0788
7	3	1	3	2	23.221	46.442	27.8652
8	3	2	1	1	27.538	64.256	34.8816
9	3	3	2	3	27.132	72.352	36.176
I	92.235	96.169	103.73	91.726			T=280.846
II	89.689	87.778	100.532	92.766			
III	98.923	96.898	76.584	96.354			
K1	30.745	32.056	34.577	30.575			
K2	29.896	29.259	33.511	30.922			
K3	32.974	32.299	25.528	32.118			
R	3.078	3.04	9.049	1.543			

surface volume of the scaffold. Three samples were measured, and the average porosity was calculated. Three samples were measured repeatedly and the average porosity was calculated.

Determination of Mechanical Properties of Scaffolds

The compression experiments of each group of scaffolds were carried out using a universal material testing machine, and the elastic modulus and compressive strength of the corresponding bracket group were calculated by taking the two-point secant slope of the strain range of 10–20%.

Preparation of Extraction Solution of Two Groups of Scaffold Materials

The two groups of scaffold materials were each cut into 5×5 mm squares. After hydrogen peroxide sterilization, the extraction medium (normal saline) was added at 6 cm^2/mL according to the sample surface area / extraction medium.[32] The scaffold extract was obtained by putting it in a 37 °C incubator (24 hours). The scaffold extract was then subjected to 4 °C for reserve.

Detection of Cytotoxicity and Adipose Stem Cells Proliferation of Scaffolds in Two Groups

Cytotoxicity and cell proliferation were detected 24 h after co-culturing the scaffold extract and Adipose stem cells (ASCs). The OD values for each group were calculated, and a bar chart was drawn according to the OD values of each group. Cell viability (%) = [OD (experimental group) − OD (blank group)] / [OD (negative group) − OD (blank group)] × 100%.

Bacteriostatic Experiment of Two Groups of Scaffolds in vitro

Three scaffolds in the control group and three in the experimental group were placed in media inoculated with Staphylococcus aureus ATCC-25923. After incubation for 24 h, the size of the bacteriostatic zone was observed.

Experimental Animal

The healthy adult male New Zealand white rabbits (36) used in this study were approximately 3 months old and weighed 2.25–2.50 kg: animal certificate number SCXK (Lu) 2016 0002, animal quarantine certificate No. 3744851078. The experimental animals were provided by the Yantai Campus of Binzhou Medical College. All animal experiments are conducted in strict accordance with the guidelines for Ethical Review of Experimental Animal Welfare of the people's Republic of China (GB/T35892-2018). And all animal experiments were approved by the Animal Experiment Committee of the Yantai Campus of the Binzhou Medical College (Yantai, China).

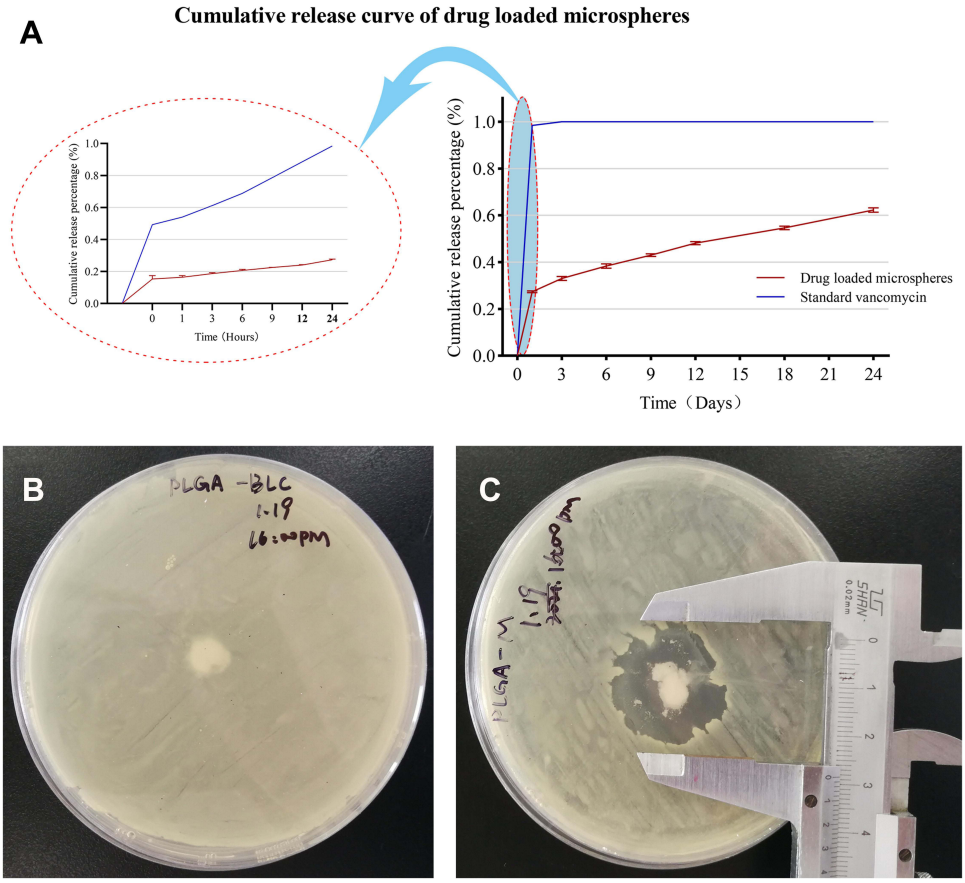

Figure 2 In vitro release and bacteriostatic activity of VAN/PLGA-MS. (**A**) Cumulative release curve of VAN/PLGA microspheres in 24 days. The picture on the left shows the cumulative release curve of 0–24 h, and the picture on the right shows the cumulative release curve of 0–24 days. (**B**) Bacteriostatic experiment of PLGA microspheres in vitro. (**C**) Bacteriostatic test of VAN/PLGA microspheres in vitro.

Experimental Animal Grouping

The experimental animals were randomly divided into three groups: blank control (group A), n-HA/LPA scaffold (group B), and VAN/MS-PLA/n-HA scaffold (group C), with 12 rabbits in each group. Group A comprised the defect model, whereas groups B and C were implanted with the two different scaffold materials to establish the bone defect model.

Construction of Bone Defect Model and Scaffold Implantation in Experimental Animals

The one-third proximal greater trochanter of the femur was located, and the fenestration area was approximately 10×3 mm. Group A included only the defect model. Group B was implanted with the n-HA/LPA scaffold, and group C was implanted with the VAN/MS-PLA/n-HA scaffold.

Observation of Gross View, X-Ray, Computed Tomography and Three-Dimensional Reconstruction After Operation

Femur specimens were collected 4, 8, and 12 weeks after surgery. After observing the gross view, X-ray films and computed tomography (CT) were used to observe the details.

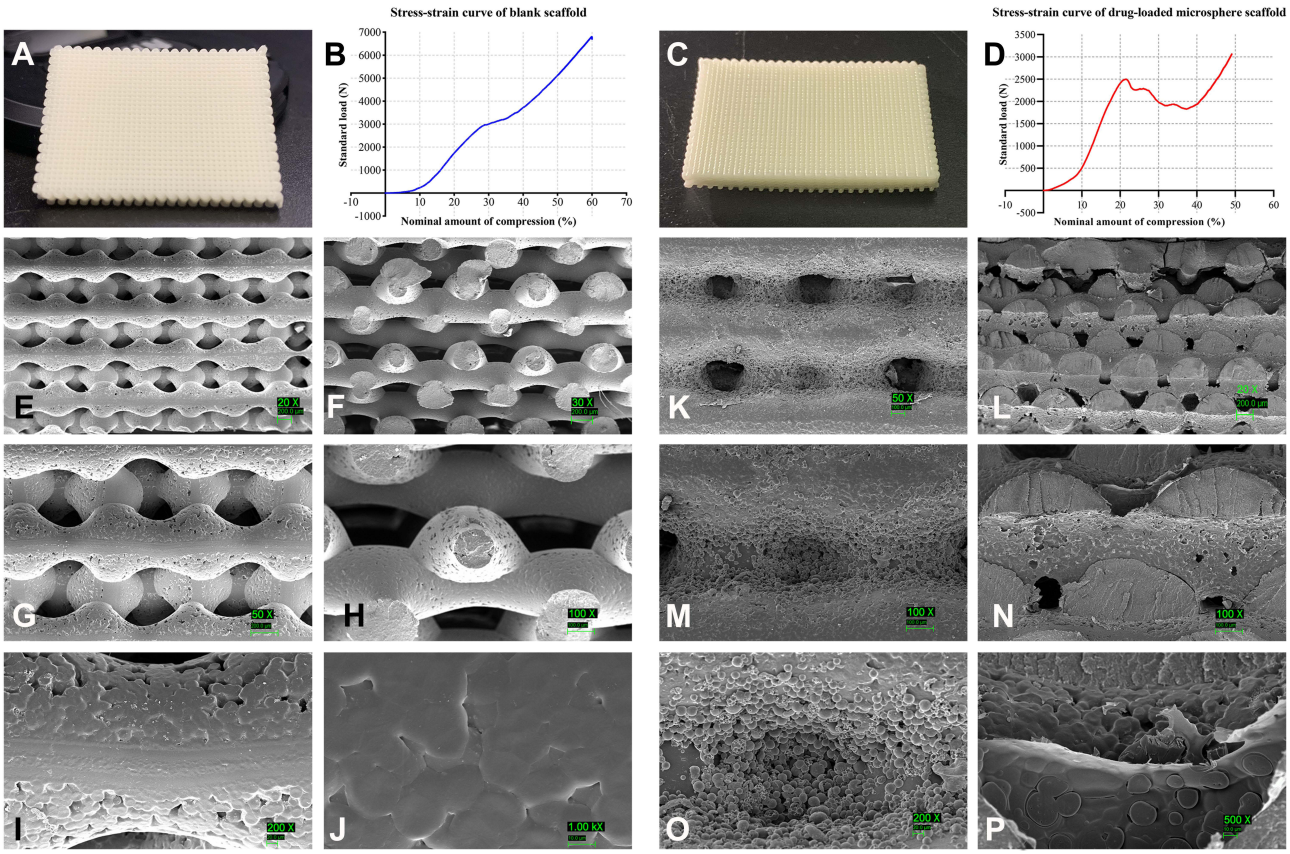

Figure 3 Characterisation of two groups of scaffolds. (**A** and **B**) General view and stress–strain curve of n-HA/PLA scaffold. (**C** and **D**) General view and stress–strain curve of VAN/MS-PLA/n-HA scaffold. (**E–J**) SEM images of n-HA/PLA scaffold under various magnifications. (**K–P**) SEM images of VAN/MS-PLA/n-HA scaffold under various magnification.

Histopathological Observation of Femur in Experimental Animals

At 4, 8, and 12 weeks post-surgery, the rabbit femur specimens were collected, and sections of the specimens containing the n-HA/PLA and VAN/MS-PLA/n-HA scaffolds were removed. These specimens were observed under a microscope after Haematoxylin and Eosin (HE) staining and Masson trichromatic staining.

In vivo Toxicity Test of Laboratory Animals

At 4, 8, and 12 weeks post-surgery, liver and kidney tissues of the rabbits were taken and stained with HE to observe the toxic reactions.

Statistical Analysis

Data statistics were compiled using the SPSS 24 statistical software. Unless otherwise specified, each sample was measured three times, and the measurement data are represented by $\bar{x} \pm$ standard deviation, S. For normally distributed data, one-way ANOVA's LSD test was used for multiple comparisons of groups of means. Differences were considered statistically significant at $p < 0.05$. All figures related to the data were generated using GraphPad Prism 8.

Results and Discussion

Preparation of PLGA/VAN-MS

Studies of carrier material and preparation technology of drug-loaded sustained-release microsphere systems provide a new approach for the treatment of chronic diseases such as infections and cancer.[33,34] Drug-loaded microspheres are

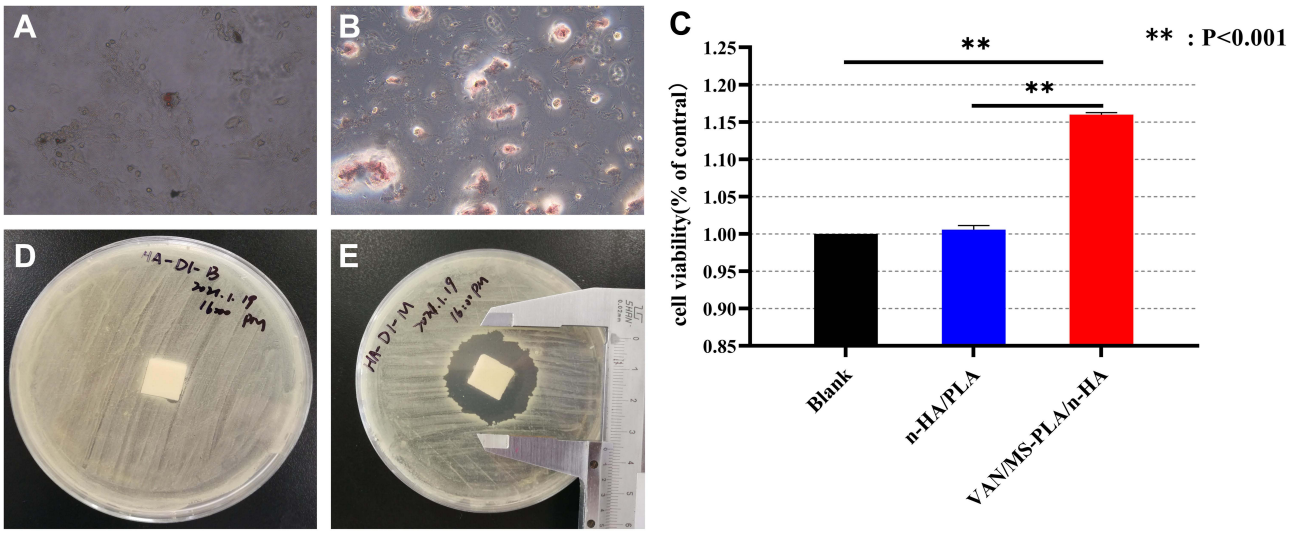

Figure 4 In vitro biological evaluation of the two groups of scaffolds. (**A**) 14 days after adipogenic induction of ASCs with Oil Red O staining under inverted microscope (100×). (**B**) 14 days after ASC osteogenic induction, alizarin red staining under inverted microscope (100×). (**C**)The effect of different scaffold on the proliferation of ASCs. (**D**) Bacteriostatic test of n-HA/PLA scaffold invitro. (**E**) Bacteriostatic experiment of VAN/MS-PLA/n-HA scaffold invitro.

spherical or quasi-spherical particles that enable drugs to dissolve in natural or synthetic materials.[35] By gathering the drug microspheres in the lesion site, the blood concentration of the lesion site can be continuously and effectively maintained above the effective bacteriostatic concentration to improve the effect of the drug, reduce the occurrence of adverse reactions, and reduce microbial drug resistance.[36] The PLGA microsphere material used in this study was a common polymer material used in microsphere carriers that is biodegradable and non-toxic to the human body.[37,38] In addition, PLGA has been recognised by the Food & Drug Administration (FDA) and the European Medicines Agency (EMA) as having good biocompatibility, degradability, and safety, and it is widely used in the study of medical engineering materials and drug delivery systems.[39–41] The VAN standard curve is shown in Figure 1A.

The equation used to determine the VAN standard curve is as follows: $Y = 0.003542 \times X + 0.005583$, $R^2 = 0.09994$. The linear relationship between 60 μg/mL and 200 μg/mL and the equation obtained in this range was used to measure the drug loading of the VAN microspheres. Because VAN is a water-soluble drug, we used 80% DE and 20% EE as the evaluation basis to achieve better drug loading. From Table 2, it can be concluded that the order of influence of the four factors is C > A > B > D. Therefore, the optimum conditions for the preparation of VAN microspheres were 500 mg of PLGA added to 9 mL of DCM, and 300 mg of VAN added to 1 mL of pure water. The concentration of the PVA solution was 2% and the speed of rotation was 1200 rpm.

The prepared microspheres resulted in a white, fine, sand-like powder that was uniformly dispersed without caking (Figure 1B). Under an electron microscope, it was observed that the microspheres were spherical (Figure 1C–F). The particle size of the PLGA/VAN-MS powder was analysed, and the results showed a normal distribution (Figure 1G). The size of the MS Dv (90) sample was 66.2 μm, indicating that 90% of the microspheres were less than 66.2 μm, which meets the expected size requirements.

Performance Evaluation of PLGA/VAN-MS

After optimising the experimental preparation process, DE% and EE% were 24.814% and 66.176%, respectively. The cumulative release curve of PLGA/VAN-MS within 24 days is shown in Figure 2A. There was an obvious sudden release on the first day, and the cumulative release rate was 27 ± 0.3%. From the second day, the drug release rate of PLGA/VAN-MS gradually decreased. On the 24th day, the cumulative drug release rate was 62.3 ± 1%. The consensus of Chinese experts on the clinical application of VAN is that the blood trough concentration of VAN in the treatment of infectious diseases should be kept above 10 μg/mL to avoid drug resistance, whereas for complex infections, such as osteomyelitis caused by Methicillin-resistant Staphylococcus aureus (MRSA), the valley concentration of vancomycin

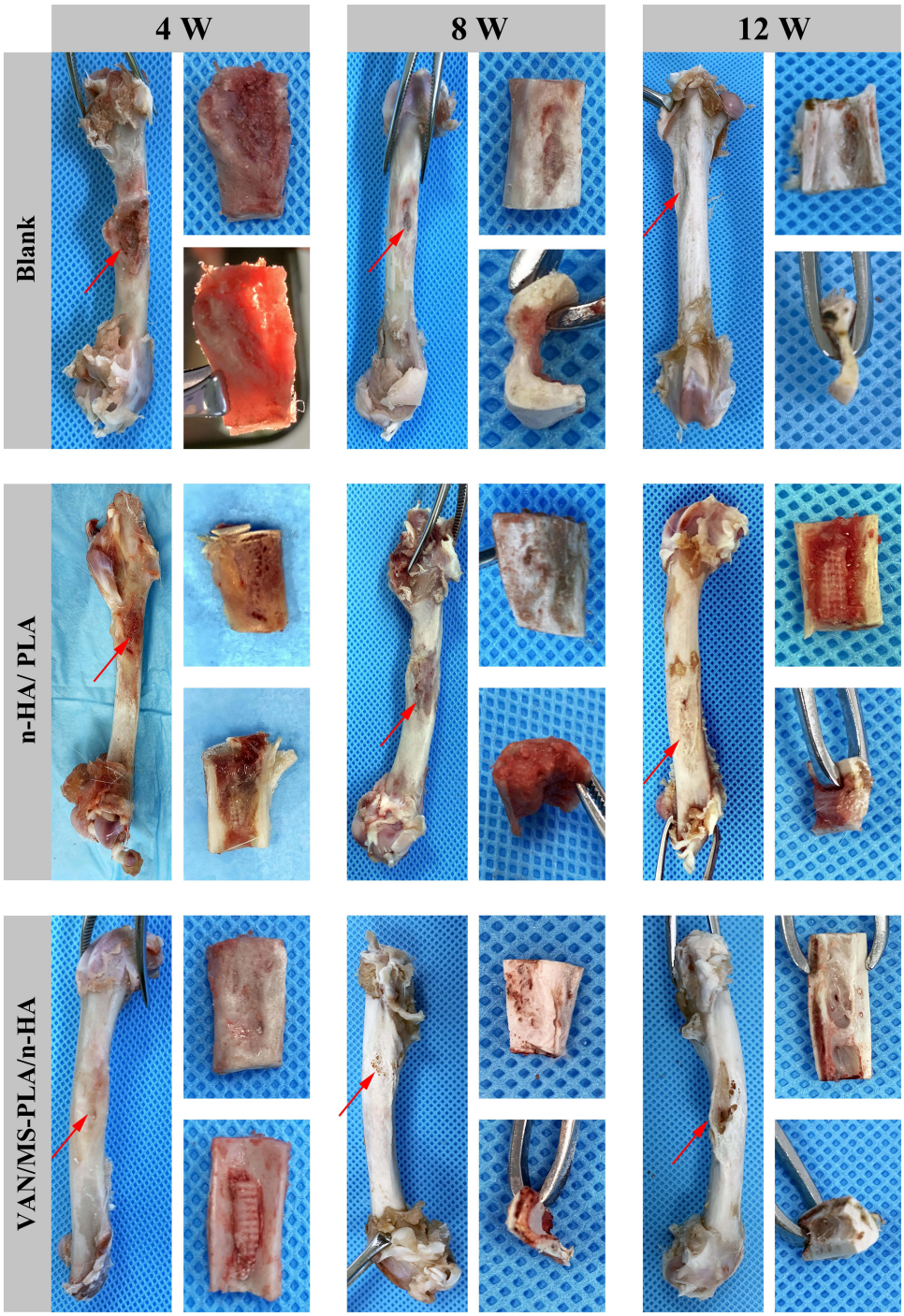

Figure 5 Femur specimens of different scaffold groups observed at 4, 8, and 12 weeks.

should be 15–20 μg/mL to achieve the treatment target and improve the clinical effectiveness.[42,43] The drug release rate of VAN/PLGA-MS prepared in this experiment was relatively stable from the second day. The average daily drug release of the 100-mg microspheres in 50 mL of PBS solution was approximately 15.75 μg/mL, which was higher than the lowest trough concentration specified in the guidelines. In addition, the bacteriostatic experiment of VAN/PLGA-MS in vitro suggested that compared with blank control microspheres without VAN (Figure 2B), the 10-mg VAN/PLGA-MS (Figure 2C) had a significant bacteriostatic effect on Staphylococcus aureus ATCC-29213 in agar medium and the effective bacteriostatic circle diameter of PLGA/VAN-MS in 24 h was approximately 2.6 ± 0.1 cm.

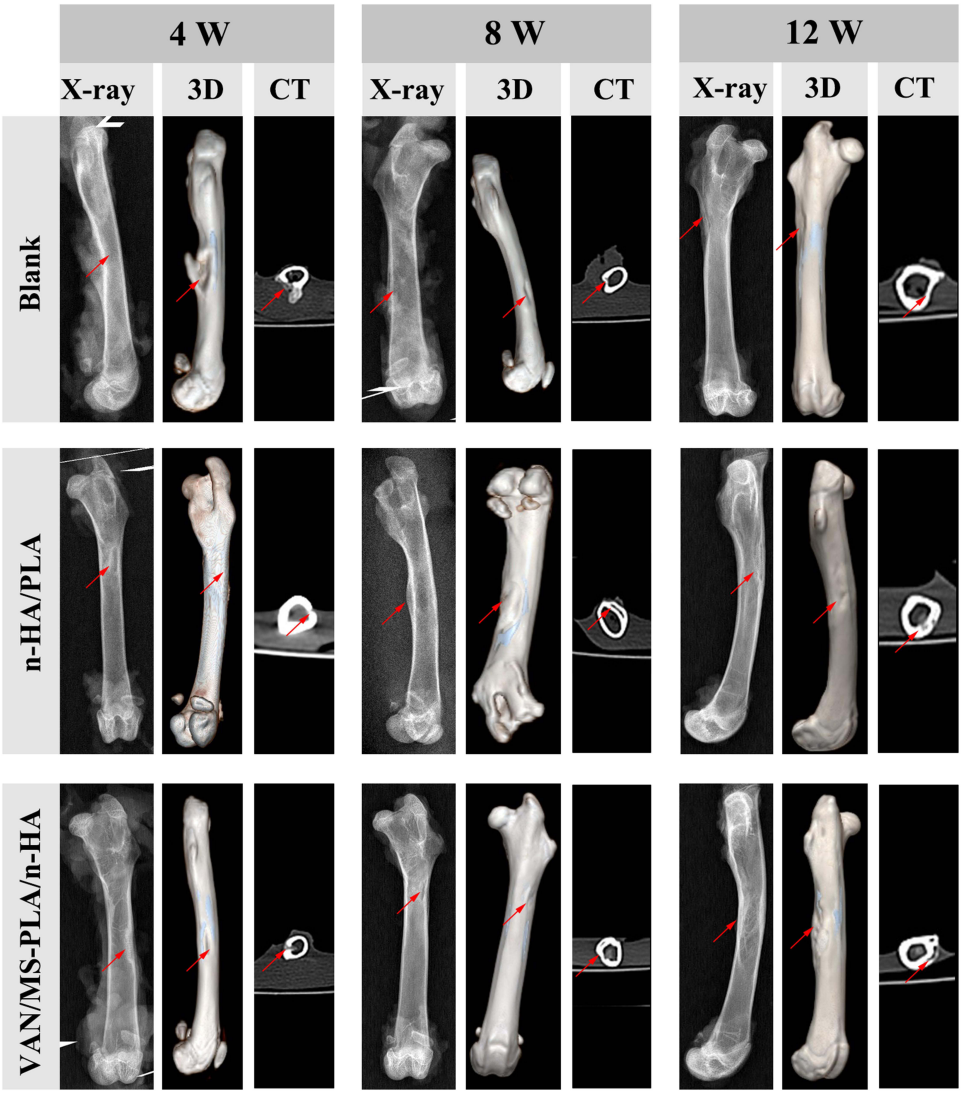

Figure 6 Femur specimens of different scaffold groups observed by X-ray, CT, and three-dimensional reconstruction at 4, 8 and 12 weeks.

Preparation and Characterization of Two Groups of Scaffolds

Although many scaffolds of different materials have been studied in vivo and in vitro, the main obstacle hindering their clinical application is the lack of vascularisation within the scaffolds, resulting in less local cytokines and weak activity in inducing osteogenesis.[44–46] In addition, the continuous emergence and proliferation of neovascularisation play an irreplaceable role in bone repair and healing. It not only provides nutrients and metabolites for defects but also provides the necessary conditions for cell proliferation and new bone regeneration.[47–49] It also participates in the regulation of cells and signal transduction during bone regeneration. A 3D printed scaffold is regarded as an ideal clinical bone substitute material because it determines the existence of controllable pores suitable for cell survival and metabolism, which results in rapid internal vascularisation and strong osteogenic activity.[50,51] The scaffold materials selected for this experiment were PLA and n-HA. PLA is a biomaterial certified by the FDA for use in the human body. It is widely used because of its good compatibility, biodegradable components, such as lactic acid, which can be excreted by the human body, and controlled degradability. As an inorganic component of bone, n-HA can significantly improve the compatibility, mechanical strength, and hydrophilicity of scaffolds. The addition of n-HA also promotes the differentiation and proliferation rate of osteocytes, resulting in excessive calcium and phosphate mineral deposits in the scaffold, which increases the formation of new bone in a short time.[52]

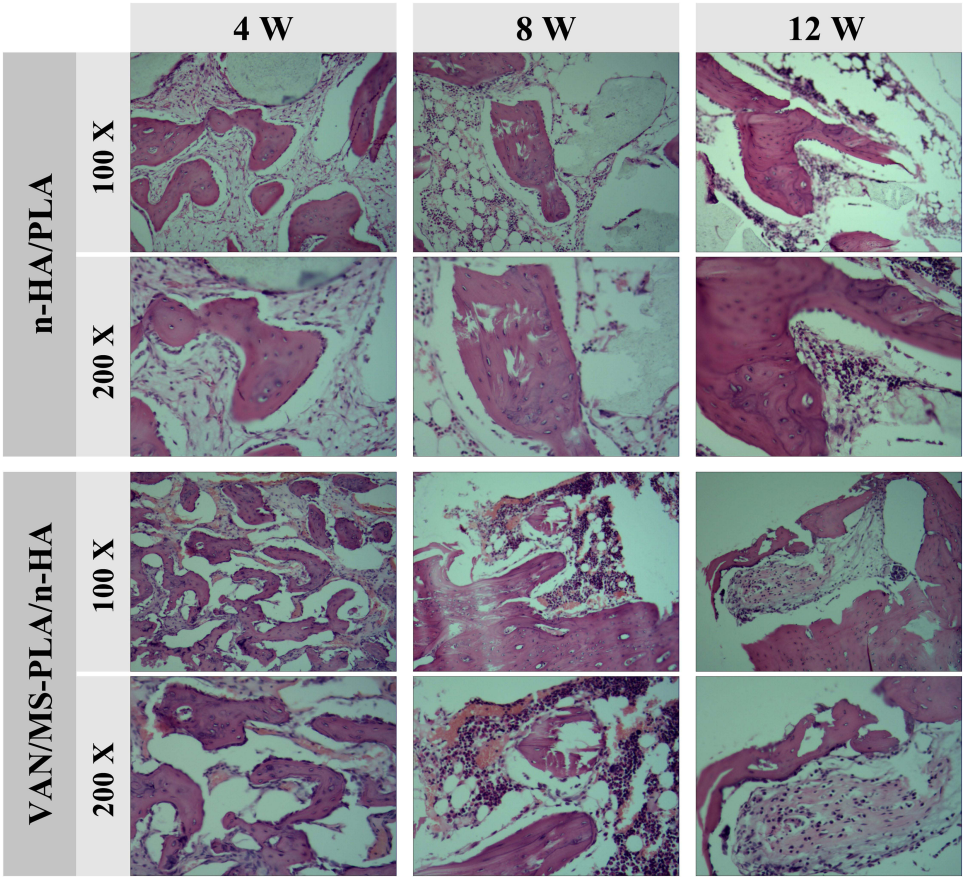

Figure 7 Histopathology of femoral defects in different scaffold groups observed at 4, 8, and 12 weeks.

The n-HA/PLA scaffold prepared in this study was a white cuboid (Figure 3A) with a print volume of 3 × 2 × 0.3 cm. SEM images showed that the print particle size was approximately 400 μm and the pore size in each layer was approximately 500 μm. The particle size was neatly arranged and uniform, and the pore size was uniform (Figure 3E–J). A uniformly distributed white powder can be seen in the pores of the VAN/MS-PLA/n-HA scaffold (Figure 3C). Under an electron microscope, multiple microspheres uniformly filling the surface and internal pores of the scaffolds were observed, and Chitosan hydrogel was visible between the microspheres to prevent them from falling off from the pores (Figure 3K–P). The porosity of the n-HA/PLA scaffold was 55.22 ± 1.009%, which is within the range of the reported porosity of bone tissue-related scaffolds (40–70%).[53–55] Within this range, the pores of the scaffolds are conducive to cell adhesion and proliferation. The stress–strain curves of the two groups of materials are shown in Figure 3B and D, respectively. The compressive strength and elastic modulus of the n-HA/PLA scaffold were 26.742 ± 1.090 MPa and 64.132 ± 3.862 MPa, respectively, and the compressive strength and elastic modulus of the VAN/MS-PLA/n-HA scaffold group were 11.490 ± 1.908 MPa and 78.235 ± 5.120 MPa, respectively. The elastic moduli of the two groups of scaffolds were thus much higher than that of human cancellous bone (2–12 MPa).[47]

Another advantage of this experiment was the CAD-aided design of the internal structure of the scaffold. Compared with the traditional immersion process, through double-nozzle 3D printing technology, the drug-loaded microspheres can be accurately and evenly distributed in the pores of the scaffold, thus avoiding their uneven distribution. With uneven distribution, the residual number of drug-loaded microspheres as the scaffold degrades is insufficient, resulting in ineffective bacteriostatic concentration.

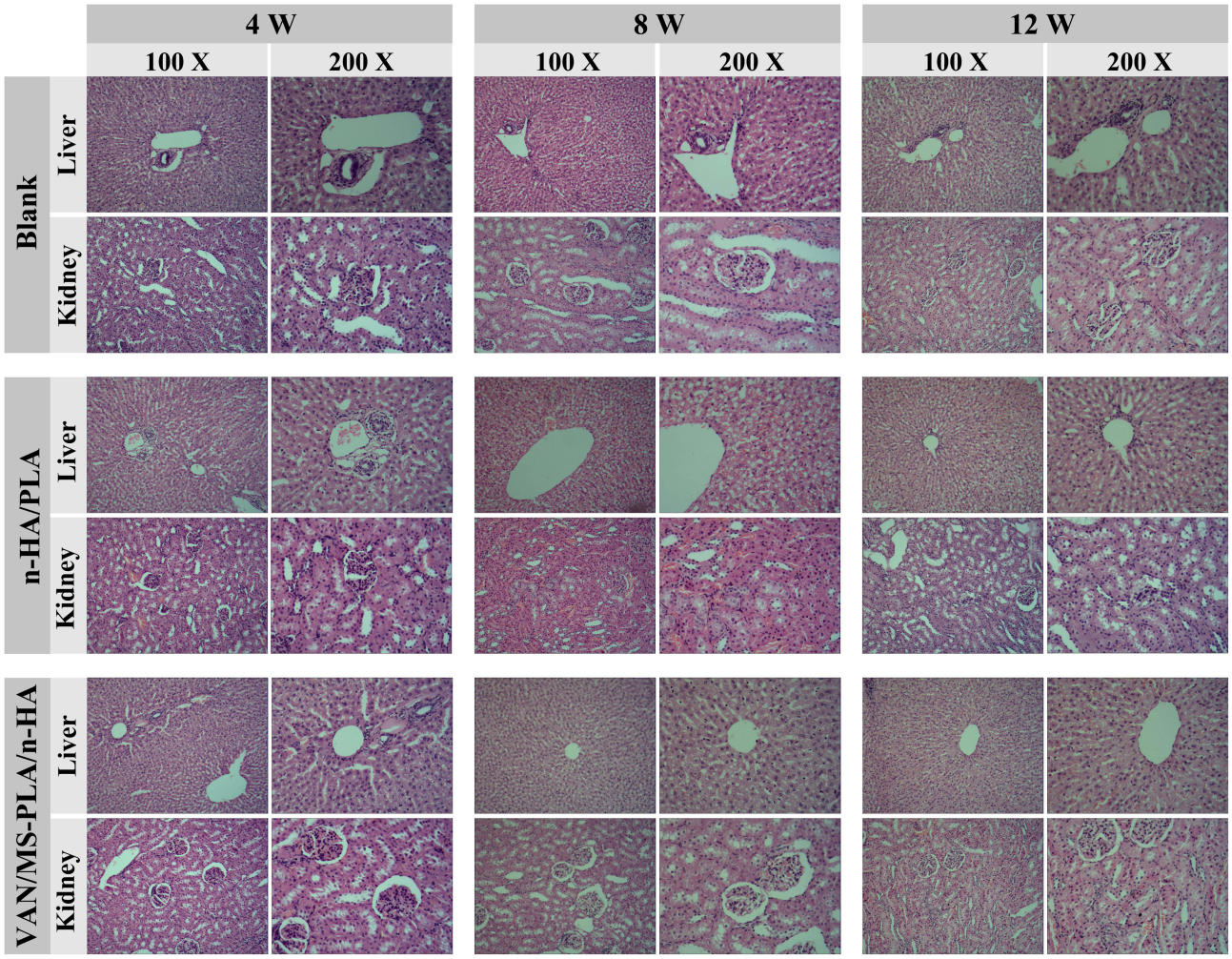

Figure 8 In vivo toxicity of experimental animals in different scaffold groups evaluated at 4, 8, and 12 weeks (liver and kidney tissue).

Biological Evaluation of Two Groups of Scaffolds in vitro

After adipogenic induction of ASCs for 14 days, Oil Red O staining showed the formation of lipid droplets of different sizes in the cytoplasm of ASCs (Figure 4A). Fourteen days after the osteogenic induction of ASCs, alizarin red staining showed mineralised matrix precipitation in the cytoplasm of ASCs (Figure 4B). Next, we evaluated the effect of scaffold extracts on the proliferation of ASCs. At 24 h, the proliferation of ASCs in the n-HA/PLA and VAN/MS-PLA/n-HA scaffold groups was significantly higher than that in the control group ($P < 0.05$), and the OD value in the VAN/MS-PLA /n-HA scaffold group was significantly higher than that in the other two groups ($P < 0.05$, Figure 4C). Finally, we evaluated the antibacterial properties of the two groups of scaffolds in vitro. Compared with the n-HA/PLA scaffold (Figure 4D), the VAN/MS-PLA/n-HA scaffold had a significant bacteriostatic effect on Staphylococcus aureus ATCC-29213 in agar medium (Figure 4E). The bacteriostatic circle diameter of the VAN/MS-PLA/n-HA scaffold after 24 h was approximately 3.3 ± 0.15 cm.

Gross Observation of Postoperative Femur Specimens in Experimental Animals

The femur specimens from each group at 4, 8, and 12 weeks are shown in Figure 5. Bone healing in groups B and C was significantly better than that in group A. The scaffolds were in good contact with the bone surface, and there was no obvious inflammatory reaction, necrosis, or non-union on the bone surface. With the extension of the scaffold implantation time, the scaffold gradually degraded. The growth of new bone into the scaffold was evident.

Observation of X-Ray, CT and Three-Dimensional Reconstruction of Postoperative Femur Specimens

As shown in Figure 6, the bone mineral density of group A over time was lower than that of other parts of the femur. The edge was sharp, the growth of new bone was slow, and the healing was incomplete. Hyperosteogeny was observed in the bone defects of groups B and C; the bone mineral densities of the two groups were similar to that of the femur, the boundaries between the scaffold materials and the defects were blurred, the new bone grew well into the scaffolds, and there was no obvious rejection or inhibition of bone growth. With the continuous degradation of the scaffold, the new bone grew into the scaffold. After the scaffolds were degraded, the area of bone defect was replaced by the new bone, the defects were blurred, and the bone thickness was similar to or higher than the local thickness of the normal femur.

Histopathological Observation of Femur in Experimental Animals

As shown in Figure 7 and Figure S2, osteoblasts were closely attached to the surface of the scaffold, the space of the scaffold was full of reactive stroma, and neovascularisation, bone matrix, and other interstitial cells were evenly distributed in the reactive stroma. There was no inflammatory cell infiltration around the scaffold, and no rejection or inhibitory reaction with the bone tissue. With the extension of the scaffold implantation time, the scaffold materials of the two groups gradually degraded, and the new bone grew into the pores of the scaffold. With the continuous degradation of the scaffold, the new bone gradually replaced the scaffold, and the bone matrix gradually merged from the initial small lumps.

Evaluation of the Toxicity of Scaffolds in Experimental Animals

As shown in Figure 8, compared with group A at 4, 8, and 12 weeks post-surgery, there was no obvious cell degeneration or punctuated or focal necrosis in the HE sections of liver tissue, no obvious infiltration or expansion of inflammatory cells in the portal area, and no local clastic necrosis, bridging necrosis, or fibrous septum formation in groups B and C. Similarly, kidney HE pathological sections showed no glomerular hyperplasia, atrophy, fibrosis, tubular atrophy, epithelial cell exfoliation, necrosis, or inflammatory cell infiltration.

Conclusions

In summary, we designed and developed the innovative VAN/MS-PLA/n-HA scaffolds with a clear pore structure that are suitable for the growth, metabolism, and proliferation of cells and capillaries in the pores for the treatment of pathogenic bone defects. The VAN/PLGA microspheres exhibited sustained release. They were evenly distributed in the pores of the n-HA/PLA scaffolds by dual-nozzle 3D printing technology for releasing the drugs step by step following the degradition of scaffolds, thus achieving the dual effects of promoting the repair of bone defects and the treatment of infections. In addition, in vitro cell and animal experiments results indicated that the composite scaffolds had good compatibility, degradability, and biomechanical properties with no cytotoxicity, and thus they can promote osteogenesis, new bone repair and reconstruction of defective bone areas. We believe that further optimisation of the VAN/MS-PLA /n-HA scaffolds to improve their mechanical strength and anti-infection performance would be beneficial for developing more effective biomaterials for therapeutic purposes.

Data Sharing Statement

The raw/processed data required to reproduce these findings are available on request from the authors.

Acknowledgments

This study was supported by Taishan Scholar Project of Shandong Province, China [NO.ts20190985], and Projects of Science & Technology Innovation and development Plan in Yantai City, China [No. 2020YD073]. We also thank all those who contributed to the whole process of the experiment.

Disclosure

The authors declare that they have no competing interests in this work.

References

1. Nauth A, Schemitsch E, Norris B, et al. Critical-size bone defects: is there a consensus for diagnosis and treatment? *J Orthop Trauma*. 2018;32 (Suppl 1):S7–S11. doi:10.1097/bot.0000000000001115
2. Wu D, Chang X, Tian J, et al. Bone mesenchymal stem cells stimulation by magnetic nanoparticles and a static magnetic field: release of exosomal miR-1260a improves osteogenesis and angiogenesis. *J Nanobiotechnology*. 2021;19(1):209. doi:10.1186/s12951-021-00958-6
3. Liu Y, Wang R, Chen S, et al. Heparan sulfate loaded polycaprolactone-hydroxyapatite scaffolds with 3D printing for bone defect repair. *Int J Biol Macromol*. 2020;148:153–162. doi:10.1016/j.ijbiomac.2020.01.109
4. Wang W, Yeung KWK. Bone grafts and biomaterials substitutes for bone defect repair: a review. *Bioact Mater*. 2017;2(4):224–247. doi:10.1016/j.bioactmat.2017.05.007
5. Bonithon R, Kao AP, Fernández MP, et al. Multi-scale mechanical and morphological characterisation of sintered porous magnesium-based scaffolds for bone regeneration in critical-sized defects. *Acta Biomater*. 2021;127:338–352. doi:10.1016/j.actbio.2021.03.068
6. Baldwin P, Li DJ, Auston DA, et al. Autograft, allograft, and bone graft substitutes: clinical evidence and indications for use in the setting of orthopaedic trauma surgery. *J Orthop Trauma*. 2019;33(4):203–213. doi:10.1097/bot.0000000000001420
7. Greenwald AS, Boden SD, Goldberg VM, et al. Bone-graft substitutes: facts, fictions, and applications. *J Bone Joint Surg Am*. 2001;83:98–103. doi:10.2106/00004623-200100022-00007
8. Wang M, Li H, Yang Y, et al. A 3D-bioprinted scaffold with doxycycline-controlled BMP2-expressing cells for inducing bone regeneration and inhibiting bacterial infection. *Bioact Mater*. 2021;6(5):1318–1329. doi:10.1016/j.bioactmat.2020.10.022
9. Bai J, Wang H, Gao W, et al. Melt electrohydrodynamic 3D printed poly (ε-caprolactone)/polyethylene glycol/roxithromycin scaffold as a potential anti-infective implant in bone repair. *Int J Pharm*. 2020;576:118941. doi:10.1016/j.ijpharm.2019.118941
10. Hassani Besheli N, Mottaghitalab F, Eslami M, et al. Sustainable release of vancomycin from silk fibroin nanoparticles for treating severe bone infection in rat tibia osteomyelitis model. *ACS Appl Mater Interfaces*. 2017;9(6):5128–5138. doi:10.1021/acsami.6b14912
11. Cui Y, Liu H, Tian Y, et al. Dual-functional composite scaffolds for inhibiting infection and promoting bone regeneration. *Mater Today Bio*. 2022;16:100409. doi:10.1016/j.mtbio.2022.100409
12. Chiarello E, Cadossi M, Tedesco G, et al. Autograft, allograft and bone substitutes in reconstructive orthopedic surgery. *Aging Clin Exp Res*. 2013;25:S101–3. doi:10.1007/s40520-013-0088-8
13. Xiong R, Zhang Z, Huang Y. Identification of optimal printing conditions for laser printing of alginate tubular constructs. *J Manuf Process*. 2015;20:450–455. doi:10.1016/j.jmapro.2015.06.023
14. Zhu Y, Goh C, Shrestha A. Biomaterial properties modulating bone regeneration. *Macromol Biosci*. 2021;21(4):e2000365. doi:10.1002/mabi.202000365
15. Dimitriou R, Jones E, Mcgonagle D, et al. Bone regeneration: current concepts and future directions. *BMC Med*. 2011;9:66. doi:10.1186/1741-7015-9-66
16. Finkemeier CG. Bone-grafting and bone-graft substitutes. *J Bone Joint Surg Am*. 2002;84(3):454–464. doi:10.2106/00004623-200203000-00020
17. Spencer V, Illescas E, Maltes L, et al. Osteochondral tissue engineering: translational research and turning research into products. *Adv Exp Med Biol*. 2018;1058:373–390. doi:10.1007/978-3-319-76711-6_17
18. Zhang C, Xu G, Han L, et al. Bone induction and defect repair by true bone ceramics incorporated with rhBMP-2 and Sr. *J Mater Sci Mater Med*. 2021;32(9):107. doi:10.1007/s10856-021-06587-7
19. Shafiee A, Atala A. Printing technologies for medical applications. *Trends Mol Med*. 2016;22(3):254–265. doi:10.1016/j.molmed.2016.01.003
20. Follin B, Juhl M, Cohen S, et al. Increased paracrine immunomodulatory potential of mesenchymal stromal cells in three-dimensional culture. *Tissue Eng Part B Rev*. 2016;22(4):322–329. doi:10.1089/ten.TEB.2015.0532
21. Ho SS, Murphy KC, Binder BY, et al. Increased survival and function of mesenchymal stem cell spheroids entrapped in instructive alginate hydrogels. *Stem Cells Transl Med*. 2016;5(6):773–781. doi:10.5966/sctm.2015-0211
22. Jana S, Lerman A. Bioprinting a cardiac valve. *Biotechnol Adv*. 2015;33(8):1503–1521. doi:10.1016/j.biotechadv.2015.07.006
23. Cui H, Nowicki M, Fisher JP, et al. 3D bioprinting for organ regeneration. *Adv Healthcare Mater*. 2017;6(1):1601118. doi:10.1002/adhm.201601118
24. Hann SY, Cui H, Esworthy T, et al. Recent advances in 3D printing: vascular network for tissue and organ regeneration. *Transl Res*. 2019;211:46–63. doi:10.1016/j.trsl.2019.04.002
25. Hann SY, Cui H, Esworthy T, et al. Dual 3D printing for vascularized bone tissue regeneration. *Acta Biomater*. 2021;123:263–274. doi:10.1016/j.actbio.2021.01.012
26. Mühlberg E, Umstätter F, Kleist C, et al. Renaissance of vancomycin: approaches for breaking antibiotic resistance in multidrug-resistant bacteria. *Can J Microbiol*. 2020;66(1):11–16.
27. Ishaq H, Tariq W, Talha KM, et al. Association between high vancomycin minimum inhibitory concentration and clinical outcomes in patients with methicillin-resistant Staphylococcus aureus bacteremia: a meta-analysis. *Infection*. 2021;49(5):803–811. doi:10.1007/s15010-020-01568-4
28. Munir MU, Salman S, Javed I, et al. Nano-hydroxyapatite as a delivery system: overview and advancements. *Artif Cells, Nanomed Biotechnol*. 2021;49(1):717–727. doi:10.1080/21691401.2021.2016785
29. Ji X, Yuan X, Ma L, et al. Mesenchymal stem cell-loaded thermosensitive hydroxypropyl chitin hydrogel combined with a three-dimensional-printed poly (ε-caprolactone) /nano-hydroxyapatite scaffold to repair bone defects via osteogenesis, angiogenesis and immunomodulation. *Theranostics*. 2020;10(2):725–740. doi:10.7150/thno.39167
30. Mao Z, Li Y, Yang Y, et al. Osteoinductivity and antibacterial properties of strontium ranelate-loaded poly (lactic-co-glycolic acid) microspheres with assembled silver and hydroxyapatite nanoparticles. *Front Pharmacol*. 2018;9:368. doi:10.3389/fphar.2018.00368
31. Jadidi A, Salahinejad E, Sharifi E, et al. Drug-delivery Ca-Mg silicate scaffolds encapsulated in PLGA. *Int J Pharm*. 2020;589:119855. doi:10.1016/j.ijpharm.2020.119855
32. General Administration Of Quality Supervision I A Q O T P S R O C C N S A C. Biological evaluation of medical devices-part 12: sample preparation and reference materials [M]; 2017.
33. Floyd JA, Galperin A, Ratner BD. Drug encapsulated polymeric microspheres for intracranial tumor therapy: a review of the literature. *Adv Drug Deliv Rev*. 2015;91:23–37. doi:10.1016/j.addr.2015.04.008

34. Zhang M, Hu W, Cai C, et al. Advanced application of stimuli-responsive drug delivery system for inflammatory arthritis treatment. *Mater Today Bio*. 2022;14:100223. doi:10.1016/j.mtbio.2022.100223
35. Birk SE, Boisen A, Nielsen LH. Polymeric nano- and microparticulate drug delivery systems for treatment of biofilms. *Adv Drug Deliv Rev*. 2021;174:30–52. doi:10.1016/j.addr.2021.04.005
36. Chung MF, Chia WT, Liu HY, et al. Inflammation-induced drug release by using a pH-responsive gas-generating hollow-microsphere system for the treatment of osteomyelitis. *Adv Healthcare Mater*. 2014;3(11):1854–1861. doi:10.1002/adhm.201400158
37. Huang J, Xia X, Zou Q, et al. The long-term behaviors and differences in bone reconstruction of three polymer-based scaffolds with different degradability. *J Mater Chem B*. 2019;7(48):7690–7703. doi:10.1039/c9tb02072a
38. Fu C, Jiang Y, Yang X, et al. Mussel-inspired gold nanoparticle and PLGA/L-lysine-g-graphene oxide composite scaffolds for bone defect repair. *Int J Nanomedicine*. 2021;16:6693–6718. doi:10.2147/ijn.S328390
39. Dodda JM, Remiš T, Rotimi S, et al. Progress in the drug encapsulation of poly (lactic-co-glycolic acid) and folate-decorated poly (ethylene glycol)-poly (lactic-co-glycolic acid) conjugates for selective cancer treatment. *J Mater Chem B*. 2022;10(22):4127–4141. doi:10.1039/d2tb00469k
40. Fraguas-Sánchez AI, Torres-Suárez AI, Cohen M, et al. PLGA nanoparticles for the intraperitoneal administration of CBD in the treatment of ovarian cancer: in vitro and in ovo assessment. *Pharmaceutics*. 2020;12(5):439. doi:10.3390/pharmaceutics12050439
41. Paik J, Duggan ST, Keam SJ. Triamcinolone acetonide extended-release: a review in osteoarthritis pain of the knee. *Drugs*. 2019;79(4):455–462. doi:10.1007/s40265-019-01083-3
42. Rybak M, Lomaestro B, Rotschafer JC, et al. Therapeutic monitoring of vancomycin in adult patients: a consensus review of the American Society of Health-System Pharmacists, the Infectious Diseases Society of America, and the Society of Infectious Diseases Pharmacists. *Am J Health Syst Pharm*. 2009;66(1):82–98. doi:10.2146/ajhp080434
43. Chen BY,He LX,Hu J, et al. Consensus of Chinese experts on clinical application of vancomycin (2011 edition). *Chin J New Drugs Clin Med*. 2011;30(8):561–573.
44. Diomede F, Marconi GD, Fonticoli L, et al. Functional relationship between osteogenesis and angiogenesis in tissue regeneration. *Int J Mol Sci*. 2020;21(9):3242. doi:10.3390/ijms21093242
45. Eftekhari H, Jahandideh A, Asghari A, et al. Assessment of polycaprolacton (PCL) nanocomposite scaffold compared with hydroxyapatite (HA) on healing of segmental femur bone defect in rabbits. *Artif Cells, Nanomed Biotechnol*. 2017;45(5):961–968. doi:10.1080/21691401.2016.1198360
46. Fitzpatrick V, Martín-Moldes Z, Deck A, et al. Functionalized 3D-printed silk-hydroxyapatite scaffolds for enhanced bone regeneration with innervation and vascularization. *Biomaterials*. 2021;276:120995. doi:10.1016/j.biomaterials.2021.120995
47. Yan Y, Chen H, Zhang H, et al. Vascularized 3D printed scaffolds for promoting bone regeneration. *Biomaterials*. 2019;190–191:97–110. doi:10.1016/j.biomaterials.2018.10.033
48. Yin S, Zhang W, Zhang Z, et al. Recent advances in scaffold design and material for vascularized tissue-engineered bone regeneration. *Adv Healthcare Mater*. 2019;8(10):e1801433. doi:10.1002/adhm.201801433
49. Zhang Y, Xie Y, Hao Z, et al. Umbilical mesenchymal stem cell-derived exosome-encapsulated hydrogels accelerate bone repair by enhancing angiogenesis. *ACS Appl Mater Interfaces*. 2021;13(16):18472–18487. doi:10.1021/acsami.0c22671
50. Chia HN, Wu BM. Recent advances in 3D printing of biomaterials. *J Biol Eng*. 2015;9:4. doi:10.1186/s13036-015-0001-4
51. Genova T, Roato I, Carossa M, et al. Advances on bone substitutes through 3D bioprinting. *Int J Mol Sci*. 2020;21(19):7012. doi:10.3390/ijms21197012
52. Hassanajili S, Karami-Pour A, Oryan A, et al. Preparation and characterization of PLA/PCL/HA composite scaffolds using indirect 3D printing for bone tissue engineering. *Mater Sci Eng C Mater Biol Appl*. 2019;104:109960. doi:10.1016/j.msec.2019.109960
53. Dubey AK, Kakimoto K. Impedance spectroscopy and mechanical response of porous nanophase hydroxyapatite–barium titanate composite. *Mater Sci Eng C Mater Biol Appl*. 2016;63:211–221. doi:10.1016/j.msec.2016.02.027
54. Ramu M, Ananthasubramanian M, Kumaresan T, et al. Optimization of the configuration of porous bone scaffolds made of polyamide/hydroxyapatite composites using selective laser sintering for tissue engineering applications. *Biomed Mater Eng*. 2018;29(6):739–755. doi:10.3233/bme-181020
55. Dhiman S, Singh M, Sidhu SS, et al. Cubic lattice structures of Ti6Al4V under compressive loading: towards assessing the performance for hard tissue implants alternative. *Materials*. 2021;14(14):3866. doi:10.3390/ma14143866